Selective mechanical transfer deposition of Langmuir graphene films for high-performance silver nanowire hybrid electrodes

Article (Accepted Version)

Article

Selective mechanical transfer deposition of Langmuir graphene films for high-performance silver nanowire hybrid electrodes

Matthew Large, Sean Paul Ogilvie, Sultan Alomairy, Terence Vöckerodt, David Myles, Maria Cann, Helios Chan, Izabela Jurewicz, Alice King, and Alan B. Dalton

Langmuir, **Just Accepted Manuscript** • DOI: 10.1021/acs.langmuir.7b02799 • Publication Date (Web): 29 Sep 2017

Selective mechanical transfer deposition of Langmuir graphene films for high-performance silver nanowire hybrid electrodes

Matthew J. Large,*,† Sean P. Ogilvie,† Sultan Alomairy,‡,¶ Terence Vöckerodt,¶ David Myles,§ Maria Cann,§ Helios Chan,§ Izabela Jurewicz,¶ Alice A. K. King,† and Alan B. Dalton*,†

†*University of Sussex, Falmer, Brighton, BN1 9RH, United Kingdom*

‡*Taif University, Taif 26571, Saudi Arabia*

¶*University of Surrey, Guildford, GU2 7XH, United Kingdom*

§*M-Solv Ltd, Oxonian Park, Kidlington, Oxfordshire, OX5 1FP, United Kingdom*

E-mail: m.large@sussex.ac.uk; a.b.dalton@sussex.ac.uk

Abstract

In this work we present silver nanowire hybrid electrodes, prepared through the addition of small quantities of pristine graphene by mechanical transfer deposition from surface-assembled Langmuir films. This technique is a fast, efficient, and facile method for modifying the opto-electronic performance of AgNW films. We demonstrate that it is possible to use this technique to perform two-step device production by selective patterning of the stamp used, leading to controlled variation in the local sheet resistance across a device. This is particularly attractive for producing extremely low-cost sensors on arbitrarily large scales. Our aim is to address some of the concerns surrounding the use of AgNW films as replacements for indium tin oxide (ITO); namely the use

of scarce materials and poor stability of AgNWs against flexural and environmental degradation.

Keywords: hybrid film, Langmuir, transfer deposition, silver nanowire, graphene

Introduction

Silver nanowire (AgNW) films are well-established competitors to indium tin oxide (ITO) in traditional transparent conductive film applications.[1–7] The opto-electronic properties of AgNW films (often described in terms of sheet resistance and transmittance at 550 nm) easily match, and often exceed, those of ITO.[3,4,8,9] There are secondary benefits as well, including low-temperature solution processing methods,[10–12] low-energy patterning techniques,[2,5,13] and compatibility with existing device architectures.[14,15] This combination of properties make AgNWs an attractive material for the electronics industry.

However, some secondary issues remain unresolved. Silver, much like indium, is a rare metal and therefore suffers from scarcity concerns which drive coating prices. While the mass of silver per unit area is very low for nanowire films, the manufacture of the nanowires increases the coating cost above the raw material price. We have previously demonstrated that by addition of small quantities of graphene to low density AgNW films it is possible to achieve comparable electro-optical performance at a fraction of the cost.[16]

There are also some issues with stability of the nanowires under various conditions, including repetitive flexing of the substrate[4,17] and atmospheric exposure.[18] Both conditions lead to drift of the sheet resistance in pristine nanowire films which can be detrimental to device performance. We show that the process of adding graphene to AgNW electrodes positively influences both of these phenomena.

In this paper we demonstrate the formation of patterned silver nanowire-graphene hybrid films (referred to as AgNW:G films) by the mechanical transfer deposition technique.[19–21] We make use of commercially available materials, and characterise the influence of the ma-

terial deposition by investigating the T-R response of the hybrid films as well as studying the resistance reduction achieved. These parameters are important for developing a 'one-step' manufacturing process, since many devices require patterned electrode structures to be produced where the ratio of 'gap' to 'track' sheet resistances is high (10^3 or greater). This process is particularly attractive for producing extremely low-cost sensors on arbitrarily large scales, such as for passive RFID devices on transparent packaging.

Results and Discussion

Poly(dimethyl siloxane) (PDMS) stamps are prepared from laser-machined Kapton masters. Figure 1**a** shows an optical micrograph of a stamp being released from the master, with insets showing the morphology of the master and stamp features. The design resembles a resolution test grating with rectilinear features varying between 200 and 25 µm in size. The features are 10 µm tall in all cases.

Building on our previous work on the preparation of density-controlled graphene films,[22] Langmuir films of graphene were prepared from a commercially available graphene powder material by dispersion into acetone as a spreading solvent. The dispersion was measured by UV-Visible spectrophotometry to have a concentration of approximately $0.02\,\mathrm{mg\,ml^{-1}}$. The dispersion was added dropwise to the Langmuir trough to form a film. By compressing the film a graphene mass coverage of $\sim 2\,\mathrm{mg\,m^{-2}}$ was obtained. Figure 2**a** shows an optical micrograph of a film transferred directly to a glass substrate. A film was also deposited onto silicon for AFM analysis of the particle size distribution; an AFM height image is shown in Figure 2**b**. The histogram of particle thickness measurements in Figure 2**c** (from the image of Figure 2**b**) shows that the material produced is predominantly few-layer graphene, with a mean particle thickness of approximately 2.8 nm. However as the insets of Figure 2**c** show the sample also contains small numbers of thicker flakes, in the region of 10 to 100 nm tall.

The graphene deposition procedure is schematically illustrated in Figure 1**b**-**g**. A Lang-

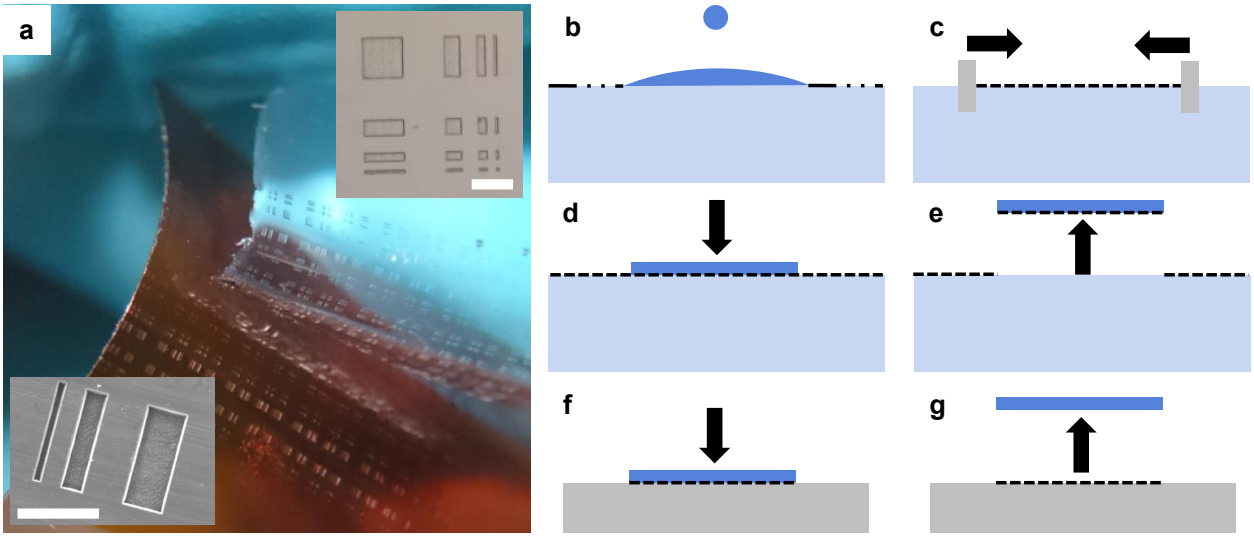

Figure 1: **a**: Optical micrograph of a PDMS stamp being released from a Kapton master. (inset) SEM micrograph of the initial master surface (bottom) and bright field optical microscope image of the produced stamp (top). **b-g**: Cartoon illustrating the film formation and deposition process. The graphene dispersion is spread on a water subphase to form a Langmuir film (**b**) which is then compressed to the desired density (**c**). The film is transferred to a PDMS stamp using the Schaefer deposition method (**d-e**), and subsequently deposited onto a substrate (**f-g**).

muir film of material is prepared at the water surface by deposition of a graphene-acetone dispersion. This film is compressed to the desired density and transferred to the PDMS stamp. Finally the stamp is brought into contact with the target substrate, and a maximised pressure of 85 kPa is applied over the contact area (see Supplementary Information for contact pressure optimisation). The stamp is removed to leave the graphene material deposited on the sample surface.

Figure 2**d-g** show films transferred using a patterned stamp (similar to that shown in Figure 1**a**) onto a set of different substrates; glass, poly(methyl methacrylate) (PMMA, Acrylic), silicon, and indium arsenide (InAs), respectively. Clearly the transfer efficiencies onto glass and PMMA are extremely poor, however the stamp pattern is very well reproduced on the silicon and InAs surfaces. This is likely due to the much larger surface free energy of the crystalline substrates,[23–26] leading to a significant decrease in the Gibbs energy of the system when a graphene flake is transferred from the stamp to the substrate. It is possible

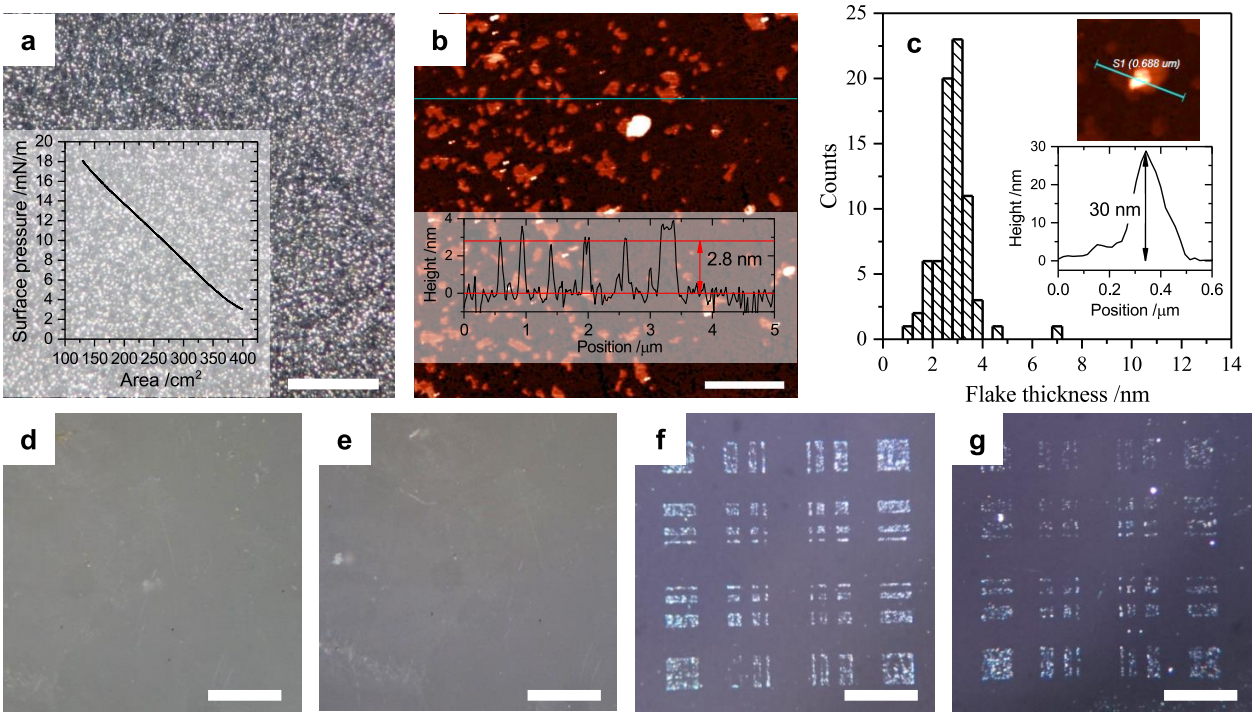

Figure 2: **a**: Optical micrograph of a L-S film of graphene deposited onto glass (the scale bar is 100 µm). (inset) Surface pressure-area isotherm for the film shown in **a**; the deposition pressure was approximately 18 mN m^{-1}. **b**: AFM height image of graphene flakes deposited on silicon (the scale bar is 1 µm). (inset) Line segment of the highlighted row in **a**, illustrating the characteristic height of the graphene flakes of ~ 3 nm. **c**: Flake thickness histogram ($N = 75$) of the AFM data in **b** showing that the material visible is on average 2.8 nm thick. (inset) AFM height data and line segment across the tall object in **b** (white object top-center), showing that the sample also contains particles with a thickness of the order of 10 to 100 nm. **d**-**g**: Optical micrographs of several substrates after patterned stamp deposition; glass (**d**), PMMA (**e**), silicon (**f**) and indium arsenide (**g**).

that there is also a contribution from surface roughness/contact intimacy effects.

A stamp design with different feature sizes was used to see whether there were any "resolution" limits to the deposition process; the stamp design is similar to a calibration grid with decreasing sizes of linear and square features. As shown in Figure 2**f** all of the features are well reproduced (where the smallest feature size is a 25 µm × 25 µm square).

There are potential applications for selective, spatially resolved nanomaterial deposition beyond those discussed in this paper. For example, controlled texture of surfaces is useful for crystal nucleation.[27] Also, graphene has been demonstrated as a material for generating terahertz radiation; the ability to selectively deposit material to produce microscale devices

may lead to integrated terahertz light sources.[28,29]

Based on our prior work it is understood that significant modification of the electro-optical properties of AgNW films can be obtained by addition of small quantities of graphene.[16] These hybrid films display sheet resistances up to five orders of magnitude lower than the pristine AgNW films with a small reduction in transmittance. In order to understand how such nanowire-graphene hybrid films might perform in devices, there are other stability considerations which we have investigated (see Figure 3).

A set of pristine AgNW films were prepared at approximately equal density ($\sim 10^5\,\Omega\,\square^{-1}$). Of these half were coated with graphene by the L-S method to achieve a final sheet resistance of $\sim 100\,\Omega\,\square^{-1}$. This approach was used to eliminate possible variability in the transfer efficiency using the mechanical deposition process. In this way we are able to compare the AgNW:G hybrids on equal terms with the pristine AgNW films.

The first such issue is the stability of AgNW films under atmospheric exposure. While in many cases this could be largely alleviated through lamination of multiple glass components in a traditional display stack (or addition of a coating layer[30]), flexible devices on polymer substrates are still susceptible to gas ingress via diffusion through the substrate. Figure S2 in the Supplementary Information compares both AgNW and AgNW:G hybrid films, prepared by L-S deposition, under atmospheric conditions in the laboratory for one month. As can be seen, the relative resistance change after one month of atmospheric exposure is three times lower for the graphene hybrid film. We anticipate that this is due to the graphene layer acting as a gas diffusion barrier for atmospheric components that cause tarnishing of silver (namely oxygen, and sulfur-containing compounds). Since the graphene layer is not continuous over the whole surface in this case, we still observe a small increase in sheet resistance ($\sim 3\,\%$) over 30 days.

A second stability issue faced by AgNW electrodes in some applications is with regards to repeated bending of the carrier substrate. It is understood that local, mechanically-induced welding of the nanowire-nanowire junctions occurs if the films are repeatedly strained,[4,31]

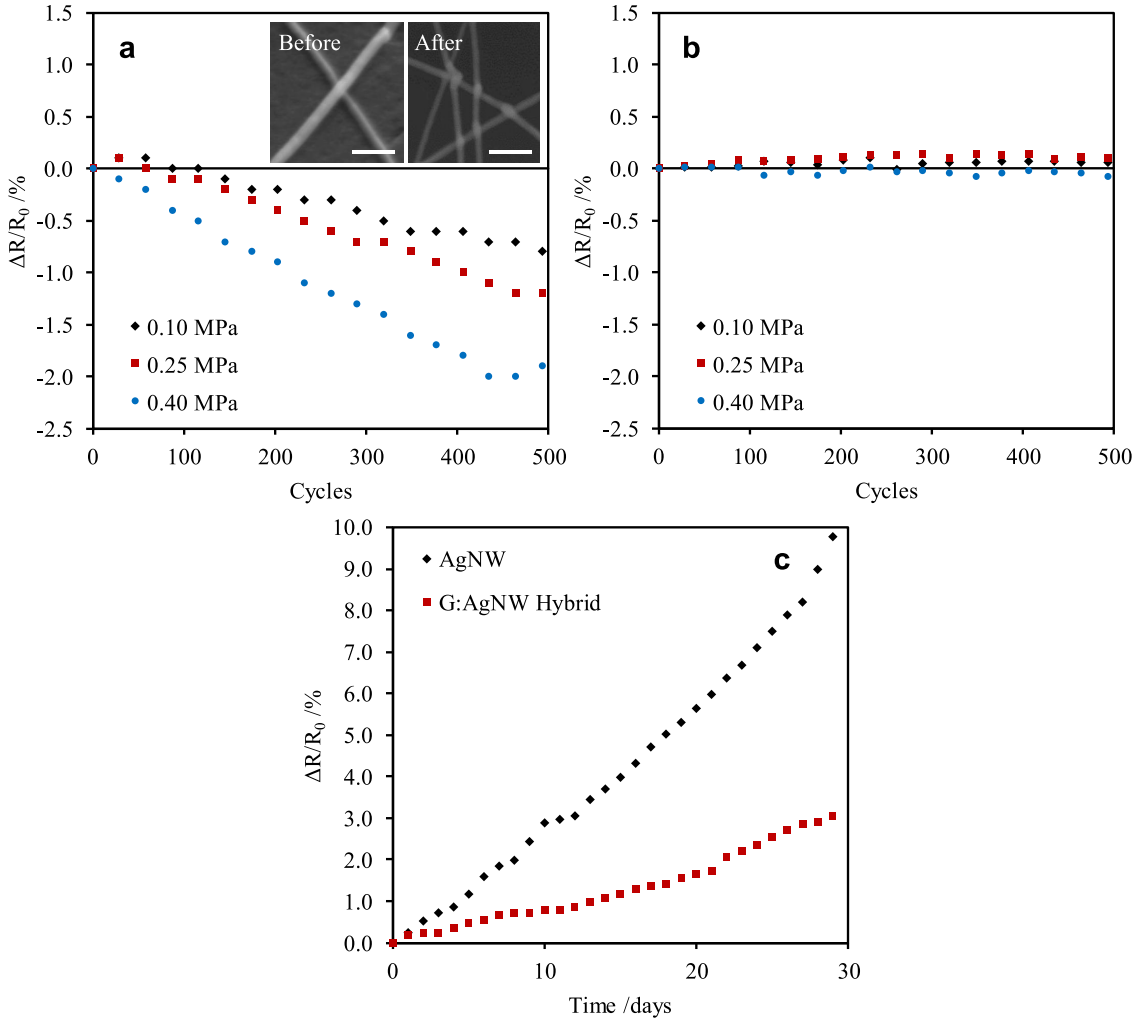

Figure 3: Variation of sheet resistance with repeated flexural cycling at increasing (decreasing) substrate stress (radius of curvature) for **a** pristine AgNW electrodes; **b** AgNW:G hybrid electrodes. (**a** inset) Representative SEM images of pristine nanowire-nanowire junctions before and after mechanical cycling. **c** Relative sheet resistance change of AgNW and AgNW:G electrodes under atmospheric exposure in the laboratory ($\sim$ 23 °C and 65 % RH) for one month.

and junction welding has been previously demonstrated to have a significant effect on the nanowire-nanowire junction resistances.[32] Over longer time scales gradual fatigue of the nanowires is also expected.[17,33] It has been demonstrated that immobilising the AgNWs (by encapsulation,[33] or improving substrate adhesion[34]) can mitigate this effect. Figure S3**a** shows the response of a pristine AgNW film to repeated flexing at three different applied stresses (corresponding to different radii or curvature). As the films are flexed at progres-

sively smaller radii of curvature we see greater decreases in sheet resistance over a fixed number of cycles. This may be considered "mechanical annealing" of the network, which may be a useful feature of nanowire electrodes in some applications. Figure S3**b** shows comparable measurements to those in Figure S3**a**, performed using AgNW:G hybrid films (again prepared by L-S deposition). We observe a reduction in the drift of the sheet resistance by approximately one order of magnitude after the addition of graphene. In capacitive sensing applications, where measurements of the device capacitance relative to its baseline self-capacitance are used to determine interaction events, drift in the film properties may compromise device performance without periodic self-calibration.

We anticipate that the above properties translate directly to films prepared by the present mechanical transfer deposition approach. In order to compare the relative changes in electro-optical performance of L-S and mechanical transfer-prepared AgNW:G hybrid films we fit transmittance-sheet resistance (T-R) data for L-S AgNW:G films[16] using the T-R model presented previously[35] (equation (1) below). The data are shown in Figure 4**a**.

$$T = 10^{-\frac{Q_{ext} d \langle l \rangle}{\langle l^2 \rangle} \left[\left(\frac{M'}{R_S} \right)^{\frac{1}{m}} + \eta_{s,c} \right]} \tag{1}$$

where T is the film transmittance at 550 nm; Q_{ext} is the extinction efficiency of the nanowires calculated from Mie theory[14] (0.56 for the nanowires used by Jurewicz et al.[16] and 0.20 for those used in the present work); d is the nominal nanowire diameter (45 nm and 25 nm, respectively); R_S is the film sheet resistance; $\eta_{s,c} = 5.6372...$ is the percolation threshold filling factor for randomly oriented rods in 2D.[36] The fitting parameters are the statistic of the length distribution of nanowires, $\langle l^2 \rangle / \langle l \rangle$; the percolation conductivity exponent m (variously symbolised n or μ in the percolation literature); a 'material constant' M', which is correlated with the junction resistance between nanowires. For each data set a delete-one jackknife procedure was used to obtain fit parameter uncertainties.[35]

The table of fit parameters inset in Figure 4**a** shows that both M' and m increase with

the addition of graphene; in keeping with the mechanism proposed by Jurewicz et al.[16] The conductive particles introduce additional inter-nanowire connections to the network, as well as compressing existing nanowire-nanowire junctions. This causes the average junction resistance to increase (since nanowire-graphene-nanowire current paths are likely to behave comparably to graphene-graphene junctions, which have a high tunnelling barrier, and therefore high contact resistance) which is responsible for the increase in M'. The broadening of the distribution of contact resistances in the system as a result of these two effects is understood to give rise to increases in the percolation exponent for conductivity, m, from the percolation theory literature.[37]

An L-S film preparation procedure was used with a large-area flat PDMS stamp to produce a T-R data set comparable to that in Figure 2**a**; this can be seen in Figure 4**b**. By using the same fitting procedure as Figure 4**a** we can see that the parameters M' and m both decrease markedly. These changes suggest a significant fall in the average junction resistance, contrary to what is observed in the data for L-S deposited AgNW-graphene hybrids. This is likely due to the combined effects of increasing numbers of junctions, as well as the effect of mechanical compression of all nanowire-nanowire junctions by the stamp itself. We can also see that the transmittance of the samples after graphene addition increases in most cases. This is responsible for the increase in the fitted value of $\langle l^2 \rangle / \langle l \rangle$, which is dictated by the transmittance of the system at the percolation threshold;[35] the upper bound on the transmittance of a conducting nanowire film. The transmittance increase may be explained by the removal of nanowires on the surface which are not sufficiently well adhered to the substrate or the rest of the network.

In order to separate the effects of graphene addition from junction compression, comparable samples were prepared and processed using a blank stamp (with no graphene addition). For a representative sample with high initial sheet resistance ($R_S = 1.6\,\mathrm{M\Omega\,\square^{-1}}$) we observe a minimal reduction in R_S of around 18 % with a negligible change in transmittance. For the stamped AgNW:G hybrid at comparable starting sheet resistance (from Figure 4**d**),

the corresponding reduction in R_S is approximately 99.75 %.The same test performed on a low R_S sample (initially $\sim 100\,\Omega\,\square^{-1}$) yields a reduction of 1 % for the blank stamp, and a reduction of 36 % for the graphene hybrid. We clearly see that the additional conduction pathways introduced by the addition of graphene, even at relatively low densities, are the dominant contribution to the reduction in R_S for films with high sheet resistance. For films of lower sheet resistance, we believe that the relative contribution of mechanical compression is higher as the junction density and film thickness increase.

Figure 4**c** shows a graphene film transferred onto a AgNW film using the same patterning procedure as the data in Figure 2. The representative inset SEM micrograph shows a single graphene flake contacting several AgNWs. Since the average flake size is comparable to the separation of neighbouring AgNWs, the majority of graphene platelets bridge multiple nanowires. This demonstrates that we are able to control the spatial distribution of graphene platelets on a nanowire film to achieve localised modification of the electrical properties. We note that the graphene transfers to the nanowire films despite not transferring to substrates upon which we deposit the nanowire films (glass and PMMA, see Figure 2**c** and **d**). This is likely due to either local stress concentration in the stamp at the rough nanowire film surface, the significantly larger surface energy of the silver[23] (which will be more comparable to the crystalline substrates in Figure 2**d**-**e**), or both.

The data presented in Figure 4**b** is based on the deposition of an optimised coverage of graphene. Following the understanding from previous work,[16] it was anticipated that graphene platelets laying across nanowire-nanowire junctions was primarily responsible for the reduction of sheet resistance (by both electrical connectivity and a capillary force-induced compression effect). As a result, the minimum amount of graphene required to achieve an optimum film sheet resistance would be dictated by the density of nanowire-nanowire junctions and the size of the graphene platelets. Equally, in order to minimise the impact of the graphene addition on the optical properties of the hybrids, we wish to utilise as little material as possible to achieve the maximum improvement in performance.

Utilising the percolation simulation framework described in[2,14] and detailed in,[38] we can determine the junction density of a film of nanowires at arbitrary sheet resistance. At the percolation threshold (where the largest reductions in R_S are seen in the work of[16]) we find that the junction density for the nanowire material in the present study is approximately $0.1\,\mu m^{-2}$. Utilising the average flake dimensions from the AFM data of Figure 2**b** ($t = 2.8\,nm$, $L \sim 100\,nm$) and the density of graphite we arrive at a mass coverage of approximately $7\,\mu g\,m^{-2}$. Performing a similar calculation using the percolation threshold coverage for disks and randomly oriented squares in the 2D plane,[36] we can estimate the threshold for material of this thickness to be in the region of $7\,mg\,m^{-2}$. For comparison, the mass coverage of continuous monolayer graphene is approximatley $0.7\,mg\,m^{-2}$.

Based on the above mass coverage and percolation threshold for the graphene material in the present work, it is clear that percolation of the graphene particles will have a minimal effect on the hybrid film conductivity. Also, an estimate of the transmittance of a graphene film of this density is $T \approx 98 - 99\,\%$. As such there should be a negligible reduction in the AgNW film transmittance due to the graphene deposition. By optimising the material coverage in this way we can maintain compatibility with industrial requirements on T and R_S, minimise material costs for producing films, and maximise the hybrid film performance.

The production of devices requires control of the ratio of sheet resistances in the "gap" regions which separate conducting "track" areas. Typically an isolation factor ($R_S(gap)/R_S(track)$) of 10^5 is specified for commercially produced devices, but values as low as 10^3 have been suggested to be acceptable. In order to understand whether stamped graphene-AgNW hybrids are capable of obtaining sufficient isolation at useful sheet resistances we plot the resistance contrast R_{Si}/R_{Sf} as a function of R_{Si} (where R_{Si} and R_{Sf} are the initial and final sheet resistances before and after graphene deposition). This shows the obtainable isolation between tracks and gaps in a patterned design, as well as the initial sheet resistance of the nanowire film required to obtain that. The ratio of these two parameters also dictates the final track sheet resistance, which may influence the device design. The resistance contrast

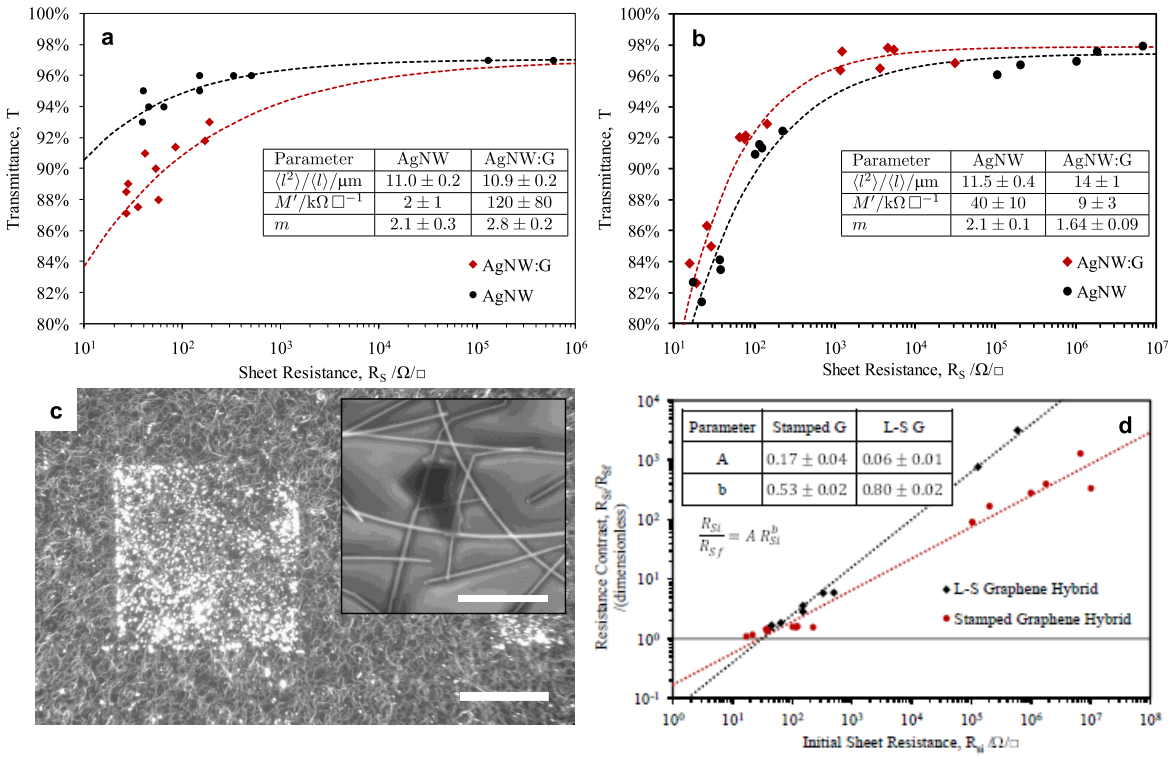

Figure 4: **a**: Transmittance-sheet resistance (T-R) data series for hybrid films prepared by direct L-S deposition (data from[16]). The series are fitted using equation (1).[35] **b**: T-R data series, equivalent to **a**, for hybrid films prepared by mechanical transfer deposition of graphene using a flat area stamp. **c**: Optical micrograph demonstrating the mechanical transfer deposition of graphene onto a silver nanowire film (scale bar 100 µm). (inset) SEM image of a graphene flake overlaying several silver nanowires (1 µm scale bar). **d**: Resistance contrast (defined as the ratio of initial to final sheet resistance) of the data sets in **a** and **c** plotted against initial film sheet resistance. The data are fitted using the inset power law expression.

for both L-S deposited and stamped graphene-AgNW hybrids is shown in Figure 4**d**.

The resistance contrast data sets are fitted with a power law expression of the form;

$$\frac{R_{Si}}{R_{Sf}} = AR_{Si}^{b} \tag{2}$$

We expect a power law dependence since the data corresponds to the ratio of two percolation-type data sets. By substituting the appropriate percolation scalings for R_{Sf} and R_{Si} into equation (2) (of the form $R_S = M'(\eta - \eta_c)^{-m}$), and allowing the percolation

thresholds to be independent in the two scaling relations, we can deduce that;

$$\eta_c(hybrid) \sim \frac{1}{m_f}\left[\left(\frac{M_i'^{1-b}}{AM_F'} - 1\right) + \eta_c\right] \tag{3}$$

By substituting the fitted parameters from Figure 4**a**, we find that the percolation threshold density (of nanowires) decreases by around 5 % for the L-S deposition process in.[16] For the present stamping deposition process, there is an increase in the percolation threshold density of approximately 30 %. This result makes intuitive sense as it suggests that the stamping process removes nanowires from the surface, but that the L-S process increases the network connectivity at very low nanowire densities. However, the result is slightly at-odds with the changes to the limiting transmittance for the hybrid films at high sheet resistance. This corresponds to the film transmittance at the percolation threshold, and so we would expect the film transmittance to decrease for the stamped hybrids based on the calculation above. The deviation possibly arises from the use of the parameters M' and m from T-R curve fits (which will be influenced by transmittance changes) along with values from resistance contrast fits (which are based on purely electrical data, and therefore cannot account for variations in transmittance).

By implementing the device design requirement that the resistance contrast be 10^3 we find for the stamped hybrids that an initial sheet resistance of $\sim 10^7\,\Omega\,\square^{-1}$ is required, using the plot in Figure 4**d**. This dictates that the final sheet resistances of the stamped AgNW:G hybrids are approximately $10^4\,\Omega\,\square^{-1}$. In the case of the L-S hybrids, however, we find that a resistance contrast of 10^3 gives initial and final sheet resistances of $10^5\,\Omega\,\square^{-1}$ and $10^2\,\Omega\,\square^{-1}$ respectively. Due to differences in graphene coverage and transfer efficiency, we anticipate that the L-S hybrid result likely represents an upper bound on what can be obtained with the mechanical transfer deposition method presented. This analysis also only considers the changes to the electrical properties of the hybrids, and there will be further considerations for the transmittance of the films and the transmittance contrast (which relates to feature

visibility to the human eye) that will impact the choice of graphene coverage when preparing hybrid films.

The study presented gives a promising proof-of-concept for device patterning based on stamped AgNW:G hybrid films. The use of large-area spray deposition to produce uniform AgNW films, and roll-to-roll coating to deposit high resistance contrast device patterns, promises a scalable, efficient, and cheap way to produce transparent opto-electronic device electrodes.

Conclusions

We have demonstrated a method for production of AgNW:G hybrid films based on mechanical transfer deposition of graphene onto spray-deposited AgNW films. These hybrid films show orders-of-magnitude decrease of sheet resistance relative to the pristine nanowire films. As well as having superior electro-optical properties, AgNW:G hybrids prepared by direct L-S deposition have been shown to have additional benefits such as stabilisation against atmospheric degradation and mechanical annealing. We believe that these properties will also be characteristic of stamped AgNW:G films, albeit dependent on the transferred graphene coverage.

Mechanical transfer deposition facilitates one-step electrode deposition, achieving levels of track-to-gap sheet resistance contrast required for device production with spatially-resolved features. Such local modification of the film properties cannot be achieved directly using L-S deposition. By optimising the deposited graphene film density, we have demonstrated resistance contrast values of approximately 10^3 with negligible change to the film transmittance.

Together these characteristics of stamped AgNW:G hybrids make them an attractive option for low-cost, scalable transparent device electrodes.

Materials and Methods

Materials

Graphene powders (Elicarb®Premium Grade Graphene Powder SP8073P) were supplied by Thomas Swan Ltd. These materials were originally prepared by high-shear exfoliation.[39] Exfoliated dispersions were processed further by the supplier; a proprietary filtration and washing approach was used to remove residual surfactant and form a powder.

The as-received powder was re-dispersed into acetone by bath ultrasonication for 1 hour (Fisher FB15051 sonic bath, nominal 300 W power output). The resulting dispersion was centrifuged at 1000 g for 1 hour to remove any irreversibly aggregated particulates. The final dispersion was measured to have a concentration of approximately $5\,\mu g\,ml^{-1}$ by UV-Vis spectroscopy (Shimadzu UV2501-PC dual beam spectrophotometer) and was used to perform Langmuir film formation without further processing.

Silver nanowires (AgNW-25) were purchased from Seashell Technologies. The as-received dispersions ($\sim 5\,mg\,ml^{-1}$) were diluted using isopropanol to a concentration suitable for spray coating, following our previous work.[2,14,16,35] Spray deposition was performed using a consumer airbrush with a commercial air compressor (Impax IM200-12L). A spraying pressure of 5 bar and nozzle-sample separation of 10 cm was used.

AgNW films were sprayed at different densities onto standard microscope slides (Fisher Scientific). Sheet resistance measurements were facilitated using a two-point geometry by applying parallel bar electrodes of silver paint (Agar Scientific G3790) with along-bar resistance of order $1\,\Omega$. Each slide was divided into three samples (a total of four electrodes per slide). Details of our film preparation process are detailed in prior publications.[2,14,16,35]

Methods

The stamp masters were made by laser ablating a polyimide film (Kapton) using the Scan Masked Imaging (SMI) process.[40] The SMI process uses a 355 nm solid state laser in a mask

imaging system to accurately machine features to 1 µm tolerances and to a uniform depth. A fluence of 1 J cm^{-2} was used to achieve an etch rate of approximately 0.5 µm/shot. The depth of the ablated feature can then be accurately tuned by varying the number of shots incident on each area. The laser machined masters were cleaned by washing with DI water followed by rinsing with IPA.

The PDMS used was a commercially available, two-part polymer/cure system (QSil 216) purchased from RS Components Ltd. The components were mixed thoroughly in a 10:1 polymer to curing agent ratio before being degassed under vacuum. The PDMS was cast onto the cleaned masters and cured in an oven at 50 °C for 60 minutes, before being released by hand.

Two types of stamp were prepared. Patterned stamps (using the laser-patterned Kapton masters, as shown in Figure 1) were cut square with a side length of approximately 5 mm. Blank stamps (used for the collection of data in Figure 4**b**) were cast from glass cover slips (22 mm × 22 mm) and cut square with a side length of approximately 20 mm.

Langmuir films of pristine graphene were prepared (using the previously described acetone-graphene dispersions) on the surface of a Nima Langmuir trough (model 602A) filled with Type 1 (18 MΩ cm resistivity) ultrapure water. A total volume in the range of 0.1 to 2 ml of solvent (depending on the desired final density) was spread over the initial trough area of 400 cm^2. Material was added drop-by-drop to the water surface, with the solvent being allowed to fully evaporate between material additions. The trough area was compressed at a rate of 20 cm^2 min^{-1} to a final area of 130 cm^2. The films were transferred using the horizontal (Schaefer) deposition method, onto either PDMS stamps or AgNW films.

The coated stamps were pressed onto the target substrate with an 85 kPa contact pressure and then removed carefully. After each deposition the stamp surface was cleaned by pressing it onto, and releasing it from, clean Scotch tape several times. This was done to remove any residual graphene, transferred nanowires, or other contaminants such as dust.

AFM measurements were performed using an NT-MDT Ntegra AFM system in semi-

contact mode, using cantilevers with a resonant frequency between 200 and 300 kHz.

Measurements of film conductivity before and after graphene deposition were made using a Keithley 2400 Sourcemeter, and UV-Vis spectroscopy (Shimadzu UV2501-PC dual beam spectrophotometer) was used to determine the change in film transmittance.

Scanning electron microscopy was performed on a Jeol JSM 7100F system. The samples were imaged without coating using an accelerating voltage of 3 kV.

Funding sources

The authors would like to gratefully acknowledge funding from M-Solv Ltd. This work was supported by the Engineering and Physical Sciences Research Council (EPSRC, grant numbers EP/K031562/1 and EP/M507775/1). The authors graciously acknowledge strategic development funding from the University of Sussex.

Acknowledgements

The authors are grateful to Dr Ronan McHale and Dr Jennifer Mackay at Thomas Swan Ltd for supplying the graphene powder used in this work.

Author contributions

Experimental concepts were devised by MJL and ABD. Laser processing was performed by DM, MC and HC. Experiments were carried out by TV, AK, MJL, SO, SA. MJL prepared the manuscript with the assistance of SO, AK, TV, IJ, ABD. DM, MC and HC reviewed the manuscript prior to submission.

References

(1) Ye, S.; Rathmell, A.; Chen, Z.; Stewart, I.; Wiley, B. Metal nanowire networks: The next generation of transparent conductors. **2014**, *26*, 6670–6687.

(2) Cann, M.; Large, M. J.; Henley, S. J.; Milne, D.; Sato, T.; Chan, H.; Jurewicz, I.; Dalton, A. B. High Performance Transparent Multi-Touch Sensors Based on Silver Nanowires. **2016**, *7*, 42–50.

(3) Bellet, D.; Lagrange, M.; Sannicolo, T.; Aghazadehchors, S.; Nguyen, V. H.; Langley, D. P.; Muñoz-Rojas, D.; Jiménez, C.; Brchet, Y.; Nguyen, N. D. Transparent Electrodes Based on Silver Nanowire Networks: From Physical Considerations towards Device Integration. **2017**, *10*, 570.

(4) Lee, J.; Lee, P.; Lee, H.; Lee, D.; Lee, S.; Ko, S. Very Long Ag Nanowire Synthesis and Its Application in a Highly Transparent, Conductive and Flexible Metal Electrode Touch Panel. *Nanoscale* **2012**, *4*, 6408–6414.

(5) Hong, S.; Yeo, J.; Lee, J.; Lee, H.; Lee, P.; Lee, S. S.; Ko, S. H. Selective Laser Direct Patterning of Silver Nanowire Percolation Network Transparent Conductor for Capacitive Touch Panel. *Journal of Nanoscience and Nanotechnology* **2015**, *15*, 2317–2323.

(6) Park, K.; Jeong, H.; Park, J.; Deressa, G.; Jeong, Y.; Lim, K.; Park, J.; Lee, S.; Kim, J. Flexible Powder Electroluminescent Device on Silver Nanowire Electrode. *Journal of Luminescence* **2015**, *165*, 216–219.

(7) Kim, H.-S.; Patel, M.; Kim, H.; Kim, J.-Y.; Kwon, M.-K.; Kim, J. Solution-Processed Transparent Conducting Ag Nanowires Layer for Photoelectric Device Applications. *Materials Letters* **2015**, *160*, 305–308.

(8) Langley, D.; Giusti, G.; Mayousse, C.; Celle, C.; Bellet, D.; Simonato, J.-P. Flexible Transparent Conductive Materials Based on Silver Nanowire Networks: A Review. *Nanotechnology* **2013**, *24*, 452001.

(9) De, S.; King, P.; Lyons, P.; Khan, U.; Coleman, J. Size Effects and the Problem with Percolation in Nanostructured Transparent Conductors. *ACS Nano* **2010**, *4*, 7064–7072.

(10) Kang, S.; Kim, T.; Cho, S.; Lee, Y.; Choe, A.; Walker, B.; Ko, S.-J.; Kim, J. Y.; Ko, H. Capillary Printing of Highly Aligned Silver Nanowire Transparent Electrodes for High-Performance Optoelectronic Devices. *Nano Letters* **2015**, *15*, 7933–7942.

(11) Park, J.; Lim, S.; Kim, H. Patterned Silver Nanowires Using the Gravure Printing Process for Flexible Applications. *Thin Solid Films* **2015**, *586*, 70–75.

(12) Finn, D.; Lotya, M.; Coleman, J. Inkjet Printing of Silver Nanowire Networks. *ACS Applied Materials and Interfaces* **2015**, *7*, 9254–9261.

(13) Spechler, J.; Arnold, C. Direct-Write Pulsed Laser Processed Silver Nanowire Networks for Transparent Conducting Electrodes. *Applied Physics A: Materials Science and Processing* **2012**, *108*, 25–28.

(14) Large, M.; Cann, M.; Ogilvie, S. P.; King, A.; Jurewicz, I.; Dalton, A. B. Finite-Size Scaling in Silver Nanowire Films: Design Considerations for Practical Devices. *Nanoscale* **2016**, *8*, 13701–13707.

(15) Park, H.-G.; Heo, G.-S.; Park, S.-G.; Jeong, H.-C.; Lee, J.; Seo, D.-S. Silver Nanowire Networks as Transparent Conducting Films for Liquid Crystal Displays. *ECS Solid State Letters* **2015**, *4*, R50–R52.

(16) Jurewicz, I.; Fahimi, A.; Lyons, P.; Smith, R.; Cann, M.; Large, M.; Tian, M.; Coleman, J.; Dalton, A. Insulator-Conductor Type Transitions in Graphene-Modified Silver

Nanowire Networks: A Route to Inexpensive Transparent Conductors. *Advanced Functional Materials* **2014**, *24*, 7580–7587.

(17) Jiang, Y.; Xi, J.; Wu, Z.; Dong, H.; Zhao, Z.; Jiao, B.; Hou, X. Highly Transparent, Conductive, Flexible Resin Films Embedded with Silver Nanowires. *Langmuir* **2015**, *31*, 4950–4957.

(18) Mayousse, C.; Celle, C.; Fraczkiewicz, A.; Simonato, J.-P. Stability of Silver Nanowire Based Electrodes under Environmental and Electrical Stresses. *Nanoscale* **2015**, *7*, 2107–2115.

(19) Xia, Y.; Whitesides, G. M. Soft Lithography. *Angewandte Chemie International Edition* **1998**, *37*, 550–575.

(20) Liang, X.; Fu, Z.; Chou, S. Y. Graphene Transistors Fabricated via Transfer-Printing In Device Active-Areas on Large Wafer. *Nano Letters* **2007**, *7*, 3840–3844.

(21) Carlson, A.; Bowen, A. M.; Huang, Y.; Nuzzo, R. G.; Rogers, J. A. Transfer Printing Techniques for Materials Assembly and Micro/Nanodevice Fabrication. *Advanced Materials* **2012**, *24*, 5284–5318.

(22) Fahimi, A.; Jurewicz, I.; Smith, R. J.; Sharrock, C. S.; Bradley, D. A.; Henley, S. J.; Coleman, J. N.; Dalton, A. B. Density Controlled Conductivity of Pristine Graphene Films. *Carbon* **2013**, *64*, 435–443.

(23) Tran, R.; Xu, Z.; Radhakrishnan, B.; Winston, D.; Sun, W.; Persson, K. A.; Ong, S. P. Surface Energies of Elemental Crystals. *Scientific Data* **2016**, *3*, sdata201680.

(24) Ozcan, C.; Hasirci, N. Evaluation of Surface Free Energy for PMMA Films. *Journal of Applied Polymer Science* **2008**, *108*, 438–446.

(25) Blass, J.; Köhler, O.; Fingerle, M.; Müller, C.; Ziegler, C. Properties and Characteristics

of Wet (HF) and Dry (RIE) Etched Borosilicate Glass. *physica status solidi (a)* **2013**, *210*, 988–993.

(26) Pehlke, E.; Moll, N.; Kley, A.; Scheffler, M. Shape and Stability of Quantum Dots. *Applied Physics A* **1997**, *65*, 525–534.

(27) Asanithi, P.; Saridakis, E.; Govada, L.; Jurewicz, I.; Brunner, E.; Ponnusamy, R.; Cleaver, J.; Dalton, A.; Chayen, N.; Sear, R. Carbon-Nanotube-Based Materials for Protein Crystallization. *ACS Applied Materials and Interfaces* **2009**, *1*, 1203–1210.

(28) Bahk, Y.-M.; Ramakrishnan, G.; Choi, J.; Song, H.; Choi, G.; Kim, Y. H.; Ahn, K. J.; Kim, D.-S.; Planken, P. C. M. Plasmon Enhanced Terahertz Emission from Single Layer Graphene. *ACS Nano* **2014**, *8*, 9089–9096.

(29) Obraztsov, P. A.; Kaplas, T.; Garnov, S. V.; Kuwata-Gonokami, M.; Obraztsov, A. N.; Svirko, Y. P. All-Optical Control of Ultrafast Photocurrents in Unbiased Graphene. *Scientific Reports* **2014**, *4*, 04007.

(30) Jin, Y.; Deng, D.; Cheng, Y.; Kong, L.; Xiao, F. Annealing-Free and Strongly Adhesive Silver Nanowire Networks with Long-Term Reliability by Introduction of a Nonconductive and Biocompatible Polymer Binder. *Nanoscale* **2014**, *6*, 4812–4818.

(31) Hwang, B.; Shin, H.-A.-S.; Kim, T.; Joo, Y.-C.; Han, S. Highly Reliable Ag Nanowire Flexible Transparent Electrode with Mechanically Welded Junctions. *Small* **2014**, *10*, 3397–3404.

(32) Bellew, A. T.; Manning, H. G.; Gomes da Rocha, C.; Ferreira, M. S.; Boland, J. J. Resistance of Single Ag Nanowire Junctions and Their Role in the Conductivity of Nanowire Networks. *ACS Nano* **2015**, *9*, 11422–11429.

(33) Jung, E.; Nam, Y.; Seo, H.; Lee, B.; Yu, J.; Lee, S.; Kim, J.-Y.; Park, J.-U.; Song, M. Highly Efficient Flexible Optoelectronic Devices Using Metal Nanowire-Conducting

Polymer Composite Transparent Electrode. *Electronic Materials Letters* **2015**, *11*, 906–914.

(34) Jang, H.; Kim, D.; Tak, H.; Nam, J.; Kim, T.-I. Ultra-Mechanically Stable and Transparent Conductive Electrodes Using Transferred Grid of Ag Nanowires on Flexible Substrate. *Current Applied Physics* **2016**, *16*, 24–30.

(35) Large, M. J.; Burn, J.; King, A. A.; Ogilvie, S. P.; Jurewicz, I.; Dalton, A. B. Predicting the Optoelectronic Properties of Nanowire Films Based on Control of Length Polydispersity. *Scientific Reports* **2016**, *6*, 25365.

(36) Mertens, S.; Moore, C. Continuum Percolation Thresholds in Two Dimensions. *Physical Review E* **2012**, *86*, 061109.

(37) Stauffer, D.; Aharony, A. *Introduction To Percolation Theory*; CRC Press, 1994.

(38) Large, M. J. Structure-Property Relationships in Silver Nanowire Coatings. doctoral, University of Surrey, 2016.

(39) Paton, K. R. et al. Scalable Production of Large Quantities of Defect-Free Few-Layer Graphene by Shear Exfoliation in Liquids. *Nature Materials* **2014**, *13*, 624–630.

(40) Myles, D. T. E.; Ziyenge, M.; Shephard, J. D.; Milne, D. C. Scanned Mask Imaging Solid State Laser Tool for Cost Effective Flip Chip – Chip Scale Package Manufacture. *Journal of Laser Micro/Nanoengineering* **2015**, *10*, 106–109.

Graphical TOC Entry